

Article

Photoelectrochemical Performance of a CuBi_2O_4 Photocathode with H_2O_2 as a Scavenger

Zohreh Masoumi ¹, Mahdi Tayebi ², S. Ahmad Masoumi Lari ³ , Bongkuk Seo ⁴, Choong-Sun Lim ⁴, Hyeon-Gook Kim ^{4,*}, Daeseung Kyung ^{1,*} and Meysam Tayebi ^{4,*}

¹ Department of Civil and Environment Engineering, University of Ulsan, Daehakro 93, Nam-gu, Ulsan 44610, Republic of Korea

² Department of Energy Engineering and Physics, Amirkabir University of Technology, Tehran 15875-4413, Iran

³ Department of Biology, York University, Farquharson Life Sciences Building, Ottawa Rd, Toronto, ON M3J 1P3, Canada

⁴ Center for Advanced Specialty Chemical, Division of Specialty and Bio-Based Chemicals Technology, Korea Research Institute of Chemical Technology (KRICT), 45 Jongguro, Ulsan 44412, Republic of Korea

* Correspondence: candoit@kRICT.re.kr (H.-G.K.); dkyung@ulsan.ac.kr (D.K.); mtayebi@kRICT.re.kr or mtayebi2900@gmail.com (M.T.)

Abstract: Photoelectrochemical (PEC) water splitting is an eco-friendly method for producing clean and sustainable hydrogen fuels. Compared with the fabrication of solar hydrogen using n-type metal oxide semiconductor photoanodes, that of solar hydrogen using p-type metal oxide semiconductor photocathodes has not been researched as thoroughly. Therefore, this study investigated the effect of drop casting time on the PEC performance of a prepared CuBi_2O_4 photocathode. XPS, HRTEM, UV-DRS, Raman spectroscopy, XRD, and SEM analyses were used to characterize the prepared CuBi_2O_4 photocathode. Owing to the high charge separation and transfer, the photocurrent density of the CuBi_2O_4 photocathode was $\sim 0.6 \text{ mA cm}^{-2}$ at 0.3 V vs. RHE. The nanoporous CuBi_2O_4 photocathode exhibited a high photocurrent density of up to 1.2 mA cm^{-2} at 0.3 V vs. RHE with H_2O_2 as a sacrificial agent. Mott–Schottky and impedance measurements were also performed on the CuBi_2O_4 photocathode to estimate its acceptor density and charge-transfer resistance.

Keywords: PEC water splitting; CuBi_2O_4 ; photocathode; charge transport; acceptor density



Citation: Masoumi, Z.; Tayebi, M.; Lari, S.A.M.; Seo, B.; Lim, C.-S.; Kim, H.-G.; Kyung, D.; Tayebi, M.

Photoelectrochemical Performance of a CuBi_2O_4 Photocathode with H_2O_2 as a Scavenger. *Inorganics* **2023**, *11*, 147. <https://doi.org/10.3390/inorganics11040147>

Academic Editor: Francis Verpoort

Received: 2 March 2023

Revised: 22 March 2023

Accepted: 29 March 2023

Published: 31 March 2023



Copyright: © 2023 by the authors. Licensee MDPI, Basel, Switzerland. This article is an open access article distributed under the terms and conditions of the Creative Commons Attribution (CC BY) license (<https://creativecommons.org/licenses/by/4.0/>).

1. Introduction

PEC water splitting is an attractive renewable energy conversion and storage method that uses sunlight to transform water into hydrogen [1–6]. In this process, n-type semiconductors are used as photoanodes for water oxidation, whereas p-type semiconductors are used as photocathodes for water reduction. Numerous p-type semiconductors, such as Cu_2O [7], GaN [8], NiO [9], and the ternary oxides CaFe_2O_4 [10], CuNb_3O_8 [11], CuFeO_2 [12], LaFeO_3 [13], and CuBi_2O_4 [14], can be applied as possible photocathode materials. Among the many p-type semiconductors, copper-based ternary oxides (CuBi_2O_4), which possess several attractive properties, are promising candidates for PEC water splitting. The favorable absorption energy bandgap of p-type CuBi_2O_4 (CBO) photocathodes, which are active in visible light, ranges between 1.5 and 1.8 eV and has received increasing attention [15–20].

CBO, a powder-type photocatalyst, has been synthesized via the hydrothermal method [21], the sol–gel method [22], solid-state synthesis [23], and metal–organic decomposition [24]. However, only a few studies have focused on fabricating a high-quality thin CBO layer with adequate electrical consistency, a high surface area, and consistent coating. Thus, developing synthesis techniques for preparing high-quality CBO electrodes would be advantageous for addressing this research gap and for enhancing their PEC water splitting.

Herein, we present a facile and economical casting for fabricating CBO photocathodes with a high surface area.

Most reported porous CBO films have an unstable structure or only partially cover the substrate [25], which typically results in low photocurrent densities. CBO films have been fabricated for PEC water splitting reactions using various synthesis techniques. However, the PEC efficiency of such films may be reduced owing to their irregular nanoporous shape. Increasing the thickness of the nanoporous thin films can minimize the exposure of the substrate to the electrolyte; however, due to restricted charge transfer, this increase in thickness may have an inverse effect on the photocurrent. A simple process for fabricating high-quality nanoporous layers is critical for developing high-performance CBO photocathodes. Herein, a simple drop casting procedure is presented with the optimization thickness of CBO films for energy conversion into PEC photovoltaics.

We optimized the effect of drop casting time on the PEC performance of the prepared $\text{CuBi}_2\text{O}_4/\text{FTO}$ thin film. The PEC performance was measured to comprehensively explore the influence of the drop casting time. Furthermore, the effect of H_2O_2 as a sacrificial agent on the CuBi_2O_4 photocathode was investigated. Mott–Schottky and electrochemical impedance (EIS) analyses were conducted to study the enhancement of the PEC performance of the CuBi_2O_4 photocathodes.

2. Experimental Section

2.1. Fabrication of CuBi_2O_4 Photocathodes' Thin Films

The substrate, fluorine-doped tin oxide-coated glass (FTO, $25\text{ mm} \times 25\text{ mm} \times 2.2\text{ mm}$, $7\text{ O}/\text{sq}$), was cleaned with deionized water, ethanol, and acetone for 15 min. Initially, 0.058 g of $\text{Cu}(\text{NO}_3)_2 \cdot 3\text{H}_2\text{O}$ was dissolved in ethanol, and 0.243 g of $\text{Bi}(\text{NO}_3)_3 \cdot 5\text{H}_2\text{O}$ was dissolved in acetic acid. Precursor solution-based drop casting processes for fabricating CuBi_2O_4 photocathodes frequently use acetic acid and ethanol as solvents to dissolve $\text{Bi}(\text{NO}_3)_3$ and $\text{Cu}(\text{NO}_3)_2$, respectively. CBO photocathodes were fabricated using a low-cost and simple drop casting method. The precursor solution ($100\text{ }\mu\text{L}$) was dropped onto FTO before being placed in a furnace (denoted as #n- CuBi_2O_4) for 5 min at $550\text{ }^\circ\text{C}$. Drop casting was performed one, two, and four more times under identical conditions, and the resulting samples were designated as #1- CuBi_2O_4 , #2- CuBi_2O_4 , and #4- CuBi_2O_4 , respectively. All CuBi_2O_4 photocathodes were calcined for 4 h at $550\text{ }^\circ\text{C}$ in a furnace. Figure 1a shows a schematic of the CuBi_2O_4 photocathode synthesis process and the procedures involved.

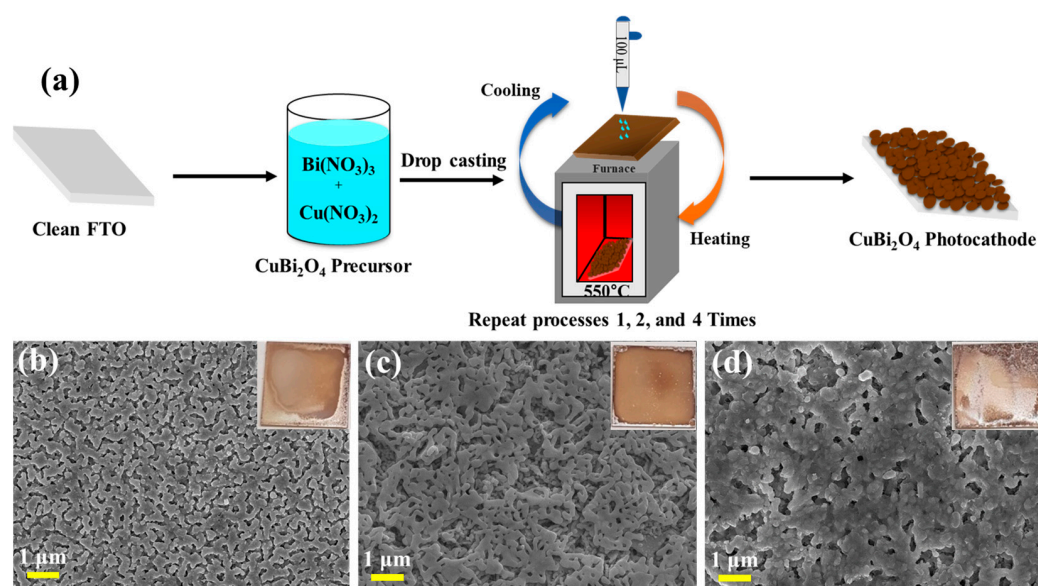


Figure 1. (a) Fabrication procedure of CuBi_2O_4 photocathodes. SEM images of CuBi_2O_4 photocathodes by the drop casting method: (b) #1- CuBi_2O_4 , (c) #2- CuBi_2O_4 , and (d) #4- CuBi_2O_4 .

2.2. Photoelectrochemical (PEC) Measurements

The synthesized CBO was utilized as the working electrode, Ag/AgCl was used as the reference electrode, and Pt wire was used as the counter electrode during the PEC measurements, which were performed in a standard three-electrode setup at a scan rate of 10 mV/s. The PEC performance was assessed in an electrolyte solution of 0.5 M Na₂SO₄ under 100 mW/cm² irradiation (AM 1.5) from the front of the photocathode using a 300 W Xe lamp. H₂O₂ was used as the electron scavenger by adding an appropriate amount of H₂O₂ to 50 mL of a 0.5M Na₂SO₄ aqueous electrolyte. A VersaSTAT 3 potentiostat was used to record the PEC characteristics, including the photocurrent, electrochemical impedance, and Mott–Schottky plots. Linear sweep voltammetry (LSV) measurements were performed at a scan rate of 0.02 Vs⁻¹. A sinusoidal voltage pulse of an amplitude of 10 mV was applied on a bias potential, with frequencies ranging from 100 kHz to 0.1Hz for the EIS of the photocathodes. The Mott–Schottky measurement was performed in the potential range of 0.7–1.6 V vs. RHE, with frequencies of 1000 Hz. The Ag/AgCl reference potential was converted into RHE using Equation (1):

$$V_{\text{RHE}} = V_{\text{Ag/AgCl}} + 0.197 + 0.059 \text{ pH} \quad (1)$$

3. Results and discussion

3.1. Physicochemical and Morphological Properties

Figure 1b shows the SEM image of a CuBi₂O₄ photocathode prepared by one-time drop casting. After one-time drop casting of the CuBi₂O₄ precursor on FTO, the CuBi₂O₄ photocathode was almost transparent and uneven (inset of Figure 1b), indicating that it was not high-quality. As shown in the inset of Figure 1c, the #2-CuBi₂O₄ photocathode became dark brown after two-time drop casting, indicating the formation of uniform nanoporous structures. After four-time drop casting (#4-CuBi₂O₄), nanoparticles agglomerated on the photocathode surface (Figure 1d). This could be one of the reasons for the lower PEC performance of the #4-CuBi₂O₄ photocathode compared with that of #2-CuBi₂O₄ [26].

Figure 2a shows the SEM image of the CuBi₂O₄ photocathode with a nanoporous structure and a nanoparticle size of ~250 nm. The effect of thickness on the PEC performances of the #1-CuBi₂O₄, #2-CuBi₂O₄, and #4-CuBi₂O₄ photocathodes was determined (Figure S5). The different drop casting processes conducted one, two, and four times (layers) led to the formation of a thin layer of CuBi₂O₄ on the substrate with thicknesses of ~450, 650, and 1000 nm, respectively. Increasing the thickness from 450 to 650 nm led to an increase in the photocurrent density. However, the photocurrent decreased when the drop casting process was repeated four times, resulting in a thickness of 1000 nm. Therefore, the best photocurrent density was obtained through the two-time drop casting processes (~650 nm) because the electron–hole pairs generated in the bulk of the films during PEC water splitting recombined before reaching the surface.

Furthermore, the HRTEM image (Figure 2b) shows CuBi₂O₄ with a nanoparticle size of ~250 nm. To illustrate the lattice spacing (the shortest distance between the planes of atoms in a crystal), HRTEM was performed using a fast Fourier transform (Figures 2c and S4). The diffraction planes of the CuBi₂O₄ lattice included 0.35 nm, which matched well with the interplanar spacing of the (211) plane of CuBi₂O₄ [15]. TEM elemental mapping showed that Cu, Bi, and O were uniformly present in the CuBi₂O₄ photocathode (Figure 2d–g).

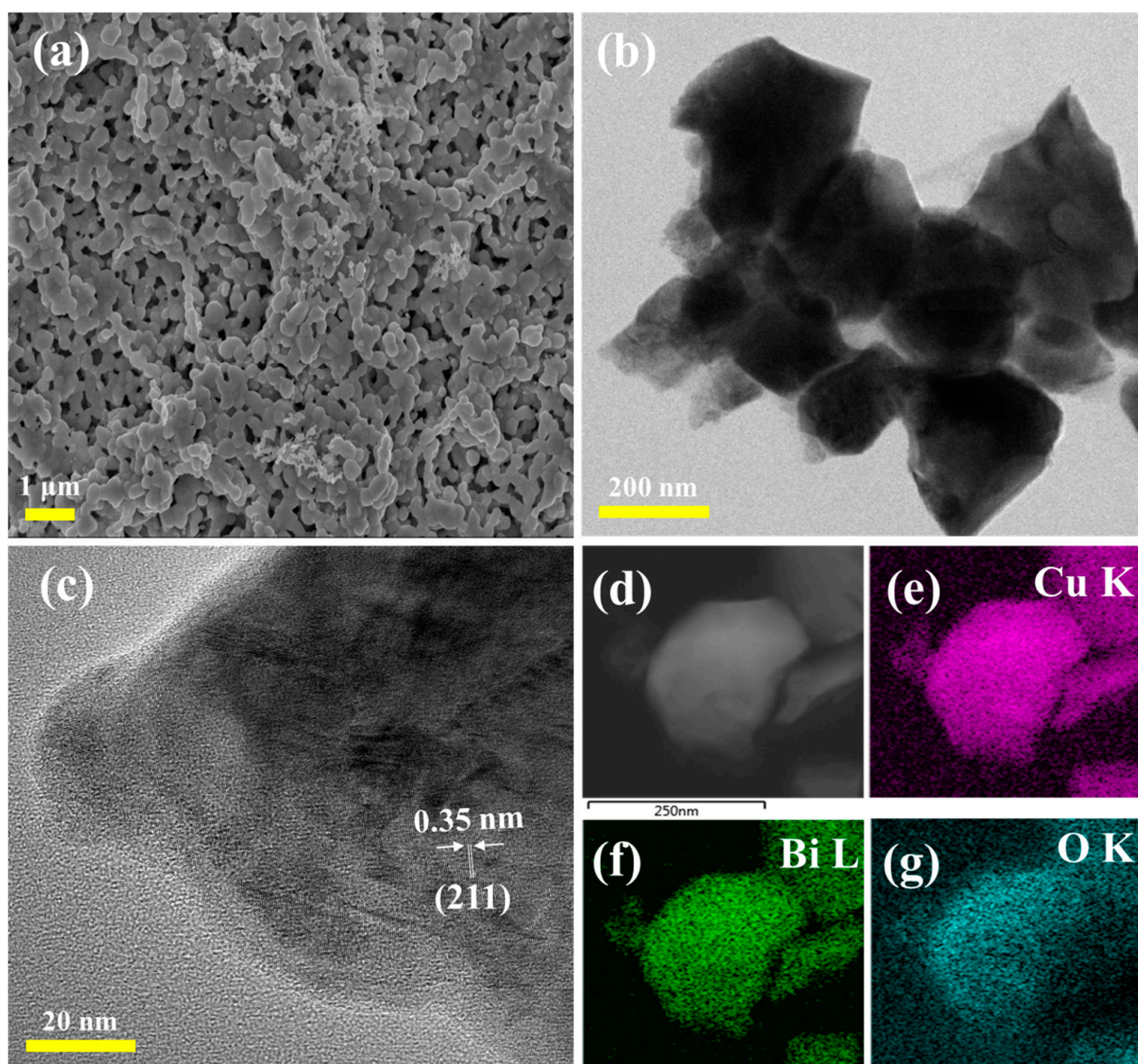


Figure 2. (a) SEM result, (b) TEM results, (c) HRTEM image of #2-CuBi₂O₄, and (d–g) TEM–EDS analysis of the #2-CuBi₂O₄ photocathode.

The XRD results confirmed the highly crystalline configuration of the photocathodes with a tetragonal structure of the CuBi₂O₄ photocathode (JCPDS No. 72–493) [27]. The Raman peaks (Figure S1) observed at 261, 404, and 587 cm^{−1} confirmed the presence of a tetragonal CuBi₂O₄ structure [21,28]. The small peak at 186 cm^{−1} was assigned to the Eg mode vibration of Cu–Cu [29]. The full-scan XPS profiles (Bi 4f, Cu 2p, and O 1s), shown in Figures 3b,c and S2, reveal that the #2-CuBi₂O₄ shows all the components in the photocathode. The Cu 2p XPS profile of the #2-CuBi₂O₄ photocathode shown in Figure S2a has two main peaks at binding energies of 933.64 and 953.4 eV that are related to Cu 2p_{3/2} and Cu 2p_{1/2}, respectively [30]. The Bi 4f XPS profile, shown in Figure 3c, has two main peaks at 158.6 and 163.9 eV, corresponding to Bi 4f_{7/2} and Bi 4f_{5/2}, respectively [31]. Furthermore, as shown in Figure S2b, the O 1s XPS profile has a main peak at 529.4 eV corresponding to lattice oxygen in metal oxides, whereas the smaller peak at 531.1 eV corresponds to the oxygen defect [32]. Figure 3d shows the UV-DRS profile of the CuBi₂O₄ photocathode. The bandgap was estimated to be 1.75 eV for the CuBi₂O₄ photocathode, consistent with the results of a previous study [17].

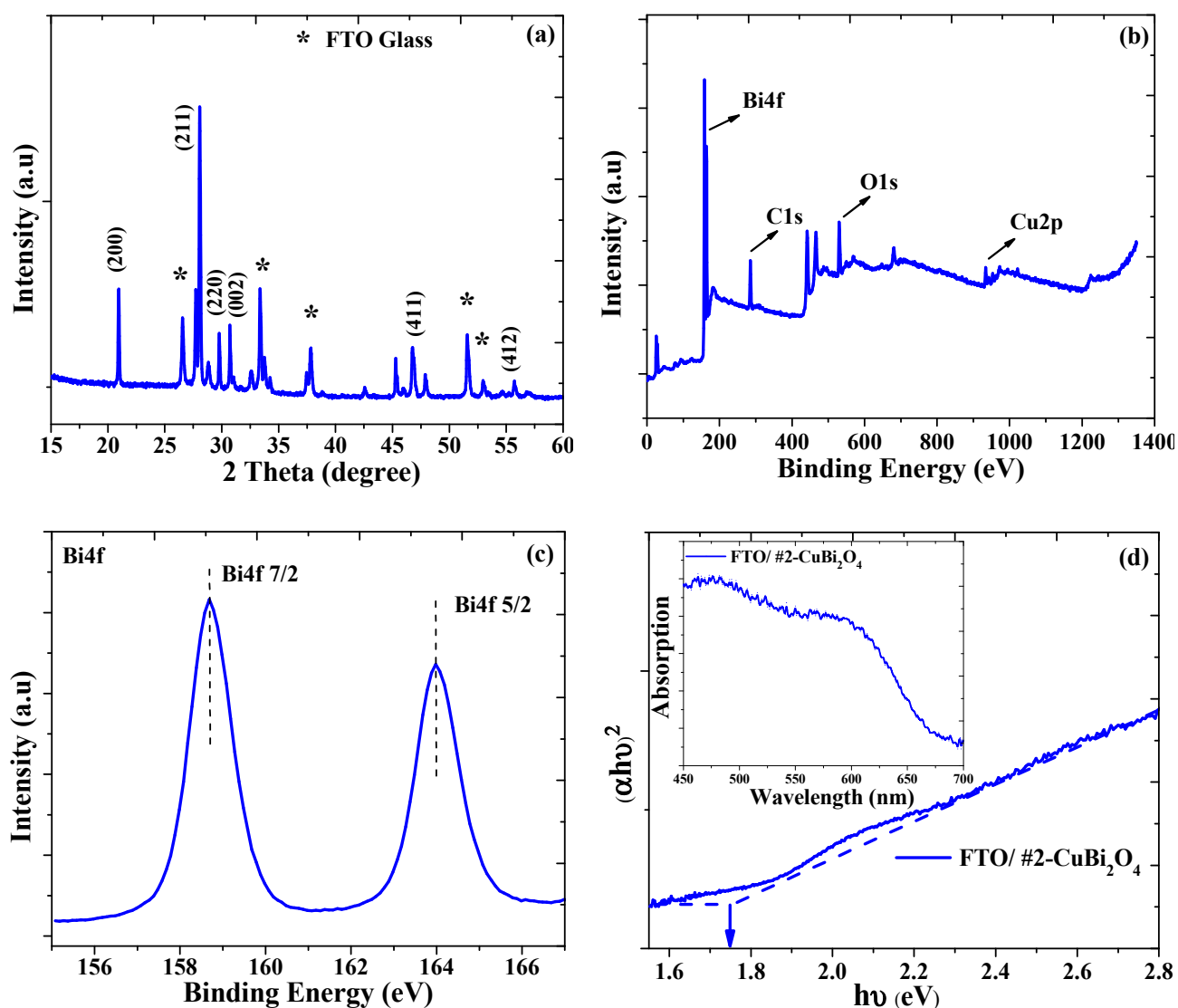


Figure 3. (a) XRD patterns, (b) XPS full-scan survey, (c) high-resolution XPS peaks for Bi 4f, and (d) band gap of the #2-CuBi₂O₄ photocathode.

3.2. PEC Water Splitting Properties

All samples exhibited negligible dark current densities (Figure 4a,b). Increasing the drop casting time led to an improvement in the photocurrent density of CuBi₂O₄. However, the photocurrent decreased after four-time drop casting. Therefore, the highest photocurrent density was achieved via two-time drop casting (#2-CuBi₂O₄ photocathode), owing to the superior electron–hole separation in the bulk of the CuBi₂O₄ photocathode during PEC water splitting.

LSV scans of #1-CuBi₂O₄, #2-CuBi₂O₄, and #4-CuBi₂O₄ are shown in Figure 4a. The LSV results indicate a p-type semiconductor in which a cathodic photocurrent was observed [33]. Figure 4a shows that the onset potentials of #1-CuBi₂O₄, #2-CuBi₂O₄, and #4-CuBi₂O₄ were ~1.05 V vs. RHE under 100 mW cm² illumination. At the optimal drop casting time (#2-CuBi₂O₄ photocathode), the photocurrent density was ~0.6 mA/cm² at 0.3 V vs. RHE. The photocurrent responses (Figure 4c,d) were in good agreement with the LSV and chopped LSV results shown in Figure 4a,b, respectively. Figure 4d shows good photocurrent stability without any significant change in the initial photocurrent for 15 min after four cycles of on–off light under 100 mW/cm² illumination.

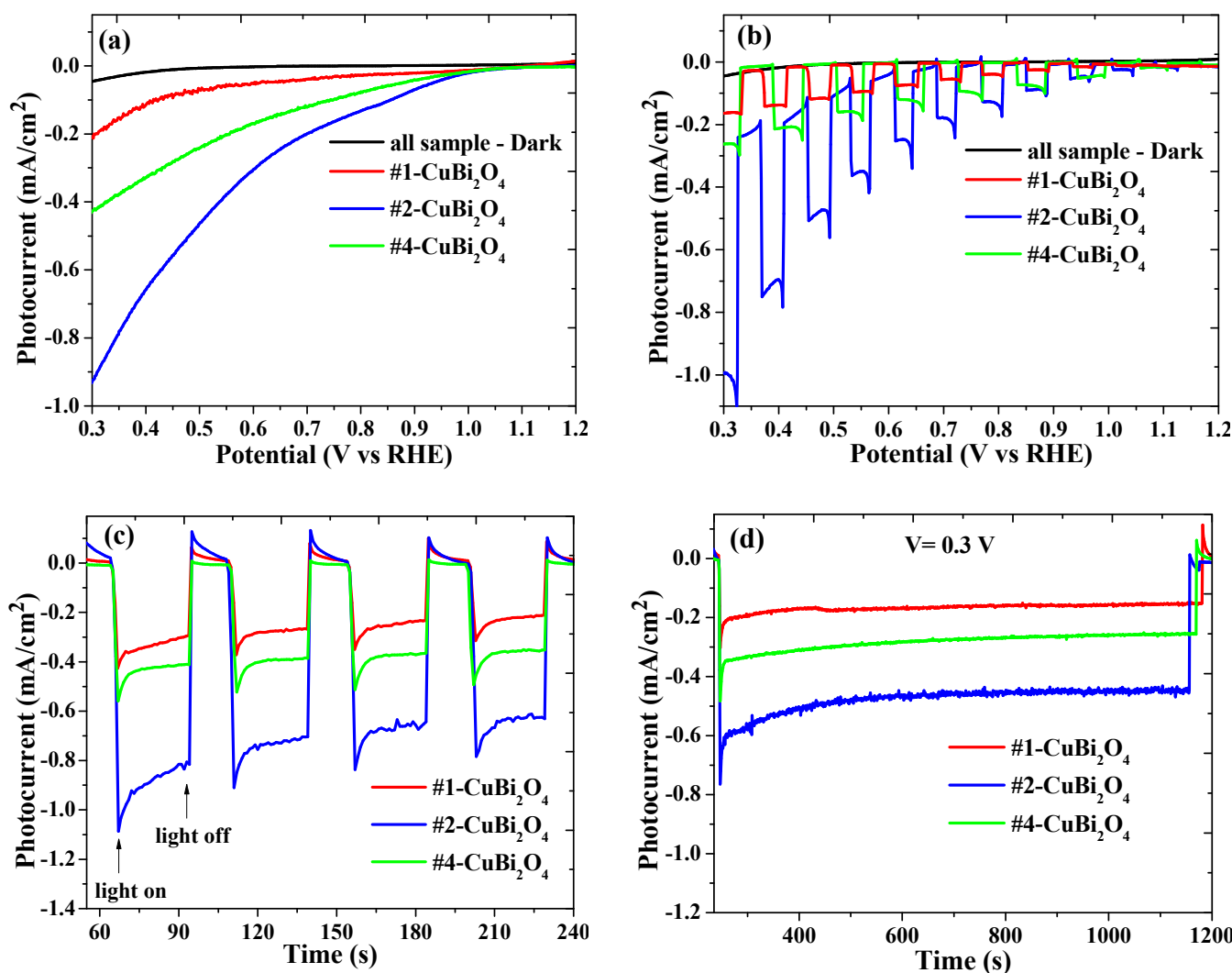


Figure 4. (a) LSV, (b) chopped LSV, (c,d) photocurrent response of the #1-CuBi₂O₄, #2-CuBi₂O₄, and #4-CuBi₂O₄ photocathodes. Under 100 mW/cm² illumination, the electrolyte was a 0.5 M aqueous solution of Na₂SO₄.

3.3. Nyquist (Impedance Analysis) and Mott–Schottky Plots

EIS was performed to study the electron–hole transport of the CuBi₂O₄ photocathodes [34,35]. The resistance of the #2-CuBi₂O₄ photocathode (R_{ct}) was determined from the radius of the semi-circle, which was smaller than that of the #1-CuBi₂O₄ and #4-CuBi₂O₄ photocathodes. The lower value of the R_{ct} for the #2-CuBi₂O₄ photocathode suggests substantially higher charge transfer properties, as shown in the Nyquist plots (Figure 5a and Table S1) [36,37]. The inset in Figure 5a shows the equivalent circuit model used in the EIS profiles. The sheet resistance (R_s), charge transfer resistance (R_{ct}), and constant phase element (CPE) correspond to those at the interface between the electrode and electrolyte, as presented in Table S1. The charge-transfer resistances of the #1-CuBi₂O₄, #2-CuBi₂O₄, and #4-CuBi₂O₄ photocathodes obtained from fitting were 1823.45, 850.37, and 1467.29 Ω /cm², respectively (Table S1), indicating a decrease in R_{ct} and the lowest arc diameter. Moreover, this suggests that the charge transport properties of these photocathodes were excellent.

Mott–Schottky measurements were performed to estimate the acceptor density (N_A) and flat band potential (V_{fb}), which are two important factors for improving the PEC performance of the #1-CuBi₂O₄, #2-CuBi₂O₄, and #4-CuBi₂O₄ photocathodes. The Mott–Schottky plots (Figure 5b) shows a negative slope for the CuBi₂O₄ photocathodes, suggesting the semiconductor’s p-type nature [38,39]. The slope of the Mott–Schottky plot was used

to calculate the acceptor density (N_A). We estimated the acceptor density (N_A) and flat band potential values from the Mott–Schottky plot (see Table S1). Further, the flat band potentials were found to be 1.34, 1.27, and 1.29 V vs. RHE for the #1-CuBi₂O₄, #2-CuBi₂O₄, and #4-CuBi₂O₄ photocathodes, respectively, which are close to the previously reported values [40–42]. The slope of #2-CuBi₂O₄ was smaller than that of the #1-CuBi₂O₄ and #4-CuBi₂O₄ photocathodes. Thus, #2-CuBi₂O₄ has a higher acceptor density, which is conducive to improving the PEC performance.

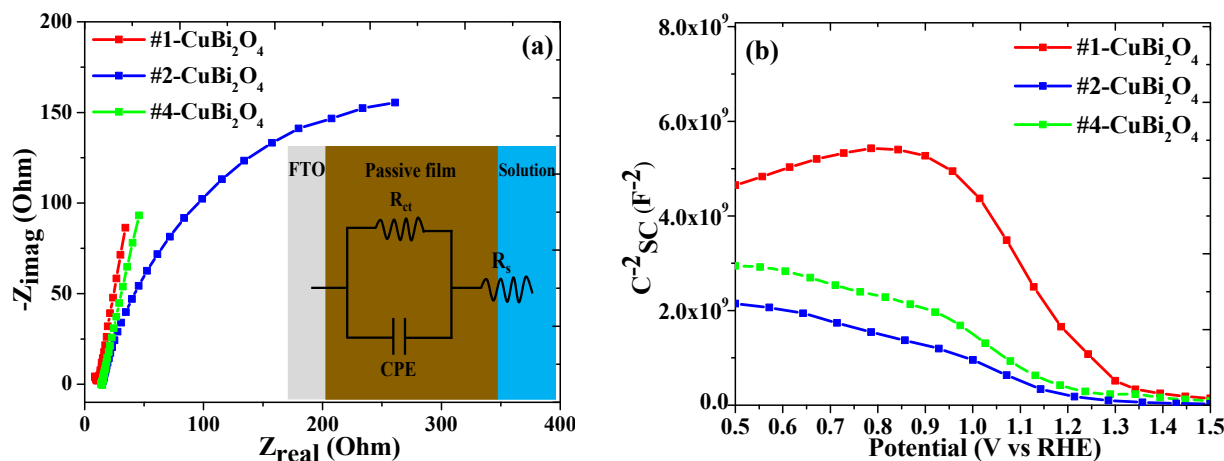


Figure 5. (a) Nyquist and (b) Mott–Schottky plots of the #1-CuBi₂O₄, #2-CuBi₂O₄, and #4-CuBi₂O₄ photocathodes. Under 100 mW/cm² illumination, the electrolyte was a 0.5 M aqueous solution of Na₂SO₄.

3.4. Effect of H₂O₂

The water splitting performance of the #2-CuBi₂O₄ photocathodes was investigated using H₂O₂ as an electron scavenger to assess their hydrogen generation capacity. H₂O₂ was added to the electrolyte as an electron scavenger to test the CuBi₂O₄ photocathodes without limitations on the reaction kinetics, which would be the case for proton reduction. In the presence of H₂O₂ as an electron scavenger, the photocurrent density can be increased to ~1.2 mA/cm² at 0.3 V vs. RHE. As shown in Figure 6a, by adding H₂O₂ (1/12.5 in volume to the electrolyte), the photocurrent increases substantially. Figure 6b shows that the semicircle for the #2-CuBi₂O₄ photocathode with H₂O₂ as a scavenger is lower than that without a scavenger, suggesting substantially superior charge transfer properties. As shown in Figure 6c, the slope of #2-CuBi₂O₄ with H₂O₂ as an electron scavenger is lower than that without a scavenger, indicating that the addition of H₂O₂ enhances the acceptor density, resulting in improved PEC performance. As an effective electron scavenger, H₂O₂ is expected to eliminate surface recombination and overcome limitations in the reaction kinetics at the semiconductor–liquid interface. The electron scavenger (H₂O₂) leads to rapid electron transfer from the CuBi₂O₄ photocathodes to H₂O₂, thereby enhancing the PEC performance [28,41,43]. Open-circuit potential analysis was performed to investigate charge carrier separation in the #2-CuBi₂O₄ photocathode with and without H₂O₂ as a scavenger. ΔOCP was higher for the #2-CuBi₂O₄ photocathode with H₂O₂ than for the #2-CuBi₂O₄ photocathode without H₂O₂ (Figure 6d). This can be attributed to the improved reaction kinetics by the suppression of recombination after light irradiation [44,45].

Figure 7 shows the complete band diagram for the CuBi₂O₄ photocathode considering the experimentally established characteristics of the UV–vis and Mott–Schottky measurements. The band diagram of the drop-deposited #2-CuBi₂O₄ photocathode is shown in Figure 7. Clearly, the valence band (VB) of CuBi₂O₄ is close to the water oxidation potential. Based on an estimated bandgap of 1.75 eV, we estimated the location of the conduction band (CB) to be ~0.48 V vs. RHE, which is more negative than the water reduction potential for hydrogen generation. In other words, the photoexcited electrons in the CB of the CuBi₂O₄ thin films can thermodynamically convert protons to hydrogen. The efficient synthesis

of H_2 by PEC water splitting requires the device to use visible light. Moreover, water is reduced on the surface of p-type semiconductor materials under visible light, whereas it is oxidized at the counter electrode.

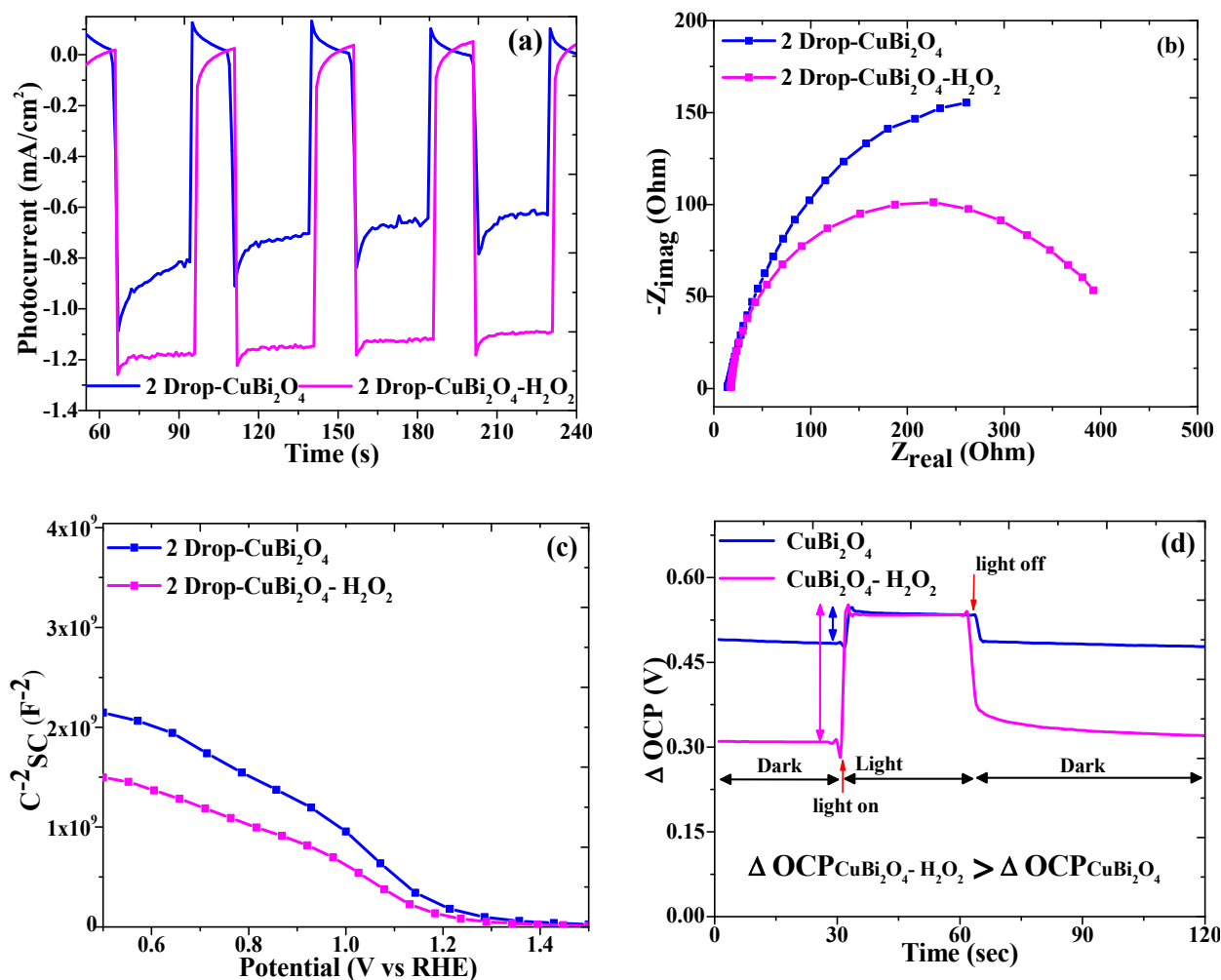


Figure 6. (a) Photocurrent response, (b) Nyquist, (c) Mott–Schottky plots, and (d) Open-circuit potential (OCP) measurements of the #2- $CuBi_2O_4$ photocathodes with and without H_2O_2 . Under 100 mW/cm^2 illumination, the electrolyte was a 0.5 M aqueous solution of Na_2SO_4 .

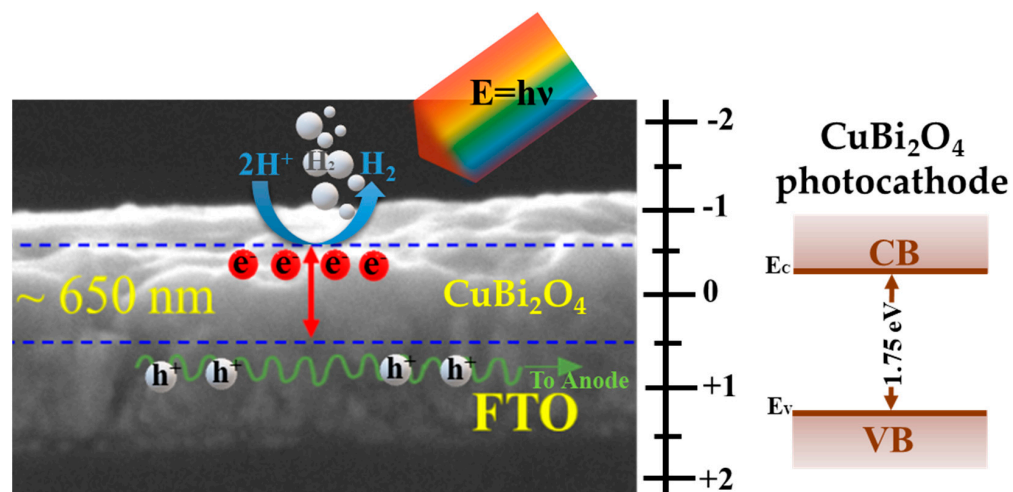


Figure 7. The mechanism and band alignment of $CuBi_2O_4$ photocathodes.

4. Conclusions

In this study, a CuBi_2O_4 photocathode was successfully prepared using a simple and low-cost drop casting method. The deposition layer was optimized using different drop casting cycles to obtain the highest photocurrent density in the CuBi_2O_4 photocathode. At the optimal time of the drop casting of the CuBi_2O_4 photocathode, the photocurrent density was $\sim 0.6 \text{ mA/cm}^2$ at 0.3 V vs. RHE under 100 mW/cm^2 illumination. The CuBi_2O_4 photocathode exhibited a high photocurrent density of up to 1.2 mA/cm^2 at 0.3 V vs. RHE with H_2O_2 as a sacrificial agent. Furthermore, Mott–Schottky and impedance measurements were performed to evaluate the acceptor density and charge transfer resistance of the CuBi_2O_4 photocathode. This study demonstrates that the semiconductors can significantly enhance the performance of metal oxide-based photocathodes toward an efficient PEC water splitting system.

Supplementary Materials: The following supporting information can be downloaded at: <https://www.mdpi.com/article/10.3390/inorganics11040147/s1>. Figure S1: Raman spectra; Figure S2: High-resolution XPS of Cu2p and O1s; Figure S3: EDX spectra of the CuBi_2O_4 photocathode; Figure S4: Inverse fast Fourier transform (IFFT) of CuBi_2O_4 ; Figure S5: SEM cross-section; Table S1: PEC parameters of the CuBi_2O_4 photocathodes.

Author Contributions: Z.M.: Writing—review & editing, Writing—original draft, Formal analysis, Investigation. M.T. (Mahdi Tayebi): Writing—original draft, Investigation. S.A.M.L.: Writing—original draft, Investigation. B.S.: Conceptualization, Supervision. C.-S.L.: Conceptualization, Supervision. H.-G.K.: Writing—review & editing, Supervision. D.K.: Writing—review & editing, Supervision. M.T. (Meysam Tayebi): Writing—review & editing, Conceptualization, Supervision. All authors have read and agreed to the published version of the manuscript.

Funding: This work was supported by the Technology Innovation Program (20011124, TS227-28R) funded by the Ministry of Trade, Industry, & Energy (MOTIE, Korea) and the KRICT core project funded by the Korea Research Institute of Chemical Technology (SS2241-10). This work was also supported by “Region-al Innovation Strategy (RIS)” through the National Research Foundation of Korea (NRF) funded by the Ministry of Education (MOE)(2021RIS-003), and the Korea Agency for Infrastructure Technology Advancement (KAIA) grant funded by the Ministry of Land, Infrastructure and Transport (Grant 23UMRG-B158194-04).

Data Availability Statement: Not applicable.

Conflicts of Interest: The authors declare no conflict of interest.

References

1. Tayebi, M.; Lee, B.-K. Recent advances in BiVO_4 semiconductor materials for hydrogen production using photoelectrochemical water splitting. *Renew. Sustain. Energy Rev.* **2019**, *111*, 332–343. [[CrossRef](#)]
2. Dashtian, K.; Shahbazi, S.; Tayebi, M.; Masoumi, Z. A review on metal-organic frameworks photoelectrochemistry: A headlight for future applications. *Coord. Chem. Rev.* **2021**, *445*, 214097. [[CrossRef](#)]
3. Raghavan, S.S.; Andrews, N.G.; Sellappan, R. Carbon-Protected BiVO_4 — Cu_2O Thin Film Tandem Cell for Solar Water Splitting Applications. *Catalysts* **2023**, *13*, 144. [[CrossRef](#)]
4. Lee, D.J.; Kumar, G.M.; Ganesh, V.; Jeon, H.C.; Kim, D.Y.; Kang, T.W.; Ilanchezhyan, P. Novel Nanoarchitected Cu_2Te as a Photocathodes for Photoelectrochemical Water Splitting Applications. *Nanomaterials* **2022**, *12*, 3192. [[CrossRef](#)]
5. Fominski, V.; Demin, M.; Fominski, D.; Romanov, R.; Rubinkovskaya, O.; Shvets, P.; Goikhman, A. Pulsed Laser Phosphorus Doping and Nanocomposite Catalysts Deposition in Forming α - $\text{MoSx}/\text{NP-Mo}/\text{n+p-Si}$ Photocathodes for Efficient Solar Hydrogen Production. *Nanomaterials* **2022**, *12*, 2080. [[CrossRef](#)]
6. Tayebi, M.; Masoumi, Z.; Seo, B.; Li, C.-S.; Kim, H.-G.; Lee, B.-K. Efficient and Stable $\text{MoOX}@\text{Mo-BiVO}_4$ Photoanodes for Photoelectrochemical Water Oxidation: Optimization and Understanding. *ACS Appl. Energy Mater.* **2022**, *5*, 11568–11580. [[CrossRef](#)]
7. Pan, L.; Kim, J.H.; Mayer, M.T.; Son, M.-K.; Ummadisingu, A.; Lee, J.S.; Hagfeldt, A.; Luo, J.; Grätzel, M. Boosting the performance of Cu_2O photocathodes for unassisted solar water splitting devices. *Nat. Catal.* **2018**, *1*, 412–420. [[CrossRef](#)]
8. Wang, X.; Yu, H.; Wu, S.; Wei, X. Field enhanced GaN photocathode and a proposed implementation method. *Optik* **2017**, *144*, 281–288. [[CrossRef](#)]
9. Hsu, C.-Y.; Chen, W.-T.; Chen, Y.-C.; Wei, H.-Y.; Yen, Y.-S.; Huang, K.-C.; Ho, K.-C.; Chu, C.-W.; Lin, J.T. Charge transporting enhancement of NiO photocathodes for p-type dye-sensitized solar cells. *Electrochim. Acta* **2012**, *66*, 210–215. [[CrossRef](#)]

10. Ida, S.; Yamada, K.; Matsunaga, T.; Hagiwara, H.; Matsumoto, Y.; Ishihara, T. Preparation of p-Type CaFe_2O_4 Photocathodes for Producing Hydrogen from Water. *J. Am. Chem. Soc.* **2010**, *132*, 17343–17345. [[CrossRef](#)]
11. Joshi, U.A.; Maggard, P.A. CuNb_3O_8 : A p-Type Semiconducting Metal Oxide Photoelectrode. *J. Phys. Chem. Lett.* **2012**, *3*, 1577–1581. [[CrossRef](#)]
12. Cheng, X.; Ding, J.; Wu, Y.; Liu, H.; Dawson, G. The photocathodic properties of a Fe_2O_3 wrapped CuFeO_2 layer on ITO glass for water splitting. *Chem. Phys.* **2018**, *513*, 241–245. [[CrossRef](#)]
13. Yu, Q.; Meng, X.; Wang, T.; Li, P.; Liu, L.; Chang, K.; Liu, G.; Ye, J. A highly durable p-La FeO_3 /n- Fe_2O_3 photocell for effective water splitting under visible light. *Chem. Commun.* **2015**, *51*, 3630–3633. [[CrossRef](#)] [[PubMed](#)]
14. Cooper, J.K.; Zhang, Z.; Roychoudhury, S.; Jiang, C.-M.; Gul, S.; Liu, Y.-S.; Dhall, R.; Ceballos, A.; Yano, J.; Prendergast, D.; et al. CuBi_2O_4 : Electronic Structure, Optical Properties, and Photoelectrochemical Performance Limitations of the Photocathode. *Chem. Mater.* **2021**, *33*, 934–945. [[CrossRef](#)]
15. Cao, D.; Nasori, N.; Wang, Z.; Mi, Y.; Wen, L.; Yang, Y.; Qu, S.; Wang, Z.; Lei, Y. p-Type CuBi_2O_4 : An easily accessible photocathodic material for high-efficiency water splitting. *J. Mater. Chem. A* **2016**, *4*, 8995–9001. [[CrossRef](#)]
16. Berglund, S.P.; Abdi, F.F.; Bogdanoff, P.; Chemseddine, A.; Friedrich, D.; van de Krol, R. Comprehensive Evaluation of CuBi_2O_4 as a Photocathode Material for Photoelectrochemical Water Splitting. *Chem. Mater.* **2016**, *28*, 4231–4242. [[CrossRef](#)]
17. Hahn, N.T.; Holmberg, V.C.; Korgel, B.A.; Mullins, C.B. Electrochemical Synthesis and Characterization of p- CuBi_2O_4 Thin Film Photocathodes. *J. Phys. Chem. C* **2012**, *116*, 6459–6466. [[CrossRef](#)]
18. Sullivan, I.; Zoellner, B.; Maggard, P.A. Copper(I)-Based p-Type Oxides for Photoelectrochemical and Photovoltaic Solar Energy Conversion. *Chem. Mater.* **2016**, *28*, 5999–6016. [[CrossRef](#)]
19. Strömberg, A.; Yuan, Y.; Li, F.; Manavaimaran, B.; Lourudoss, S.; Zhang, P.; Sun, Y. Heteroepitaxial Growth of GaP Photocathode by Hydride Vapor Phase Epitaxy for Water Splitting and CO_2 Reduction. *Catalysts* **2022**, *12*, 1482. [[CrossRef](#)]
20. MKumar; Meena, B.; Subramanyam, P.; Suryakala, D.; Subrahmanyam, C. Emerging Copper-Based Semiconducting Materials for Photocathodic Applications in Solar Driven Water Splitting. *Catalysts* **2022**, *12*, 1198.
21. Yuvaraj, S.; Karthikeyan, K.; Kalpana, D.; Lee, Y.S.; Selvan, R.K. Surfactant-free hydrothermal synthesis of hierarchically structured spherical CuBi_2O_4 as negative electrodes for Li-ion hybrid capacitors. *J. Colloid Interface Sci.* **2016**, *469*, 47–56. [[CrossRef](#)]
22. Zhang, J.; Jiang, Y.; Gao, W.; Hao, H. Synthesis and visible photocatalytic activity of new photocatalyst MBi_2O_4 (M = Cu, Zn). *J. Mater. Sci. Mater. Electron.* **2015**, *26*, 1866–1873. [[CrossRef](#)]
23. Elaziouti, A.; Laouedj, N.; Bekka, A. Synergetic effects of Sr-doped CuBi_2O_4 catalyst with enhanced photoactivity under UVA-light irradiation. *Environ. Sci. Pollut. Res.* **2016**, *23*, 15862–15876. [[CrossRef](#)] [[PubMed](#)]
24. Arai, T.; Yanagida, M.; Konishi, Y.; Iwasaki, Y.; Sugihara, H.; Sayama, K. Efficient Complete Oxidation of Acetaldehyde into CO_2 over $\text{CuBi}_2\text{O}_4/\text{WO}_3$ Composite Photocatalyst under Visible and UV Light Irradiation. *J. Phys. Chem. C* **2007**, *111*, 7574–7577. [[CrossRef](#)]
25. Xu, N.; Li, F.; Gao, L.; Hu, H.; Hu, Y.; Long, X.; Ma, J.; Jin, J. Polythiophene coated CuBi_2O_4 networks: A porous inorganic–organic hybrid heterostructure for enhanced photoelectrochemical hydrogen evolution. *Int. J. Hydrogen Energy* **2018**, *43*, 2064–2072. [[CrossRef](#)]
26. Xu, Y.; Jian, J.; Li, F.; Liu, W.; Jia, L.; Wang, H. Porous CuBi_2O_4 photocathodes with rationally engineered morphology and composition towards high-efficiency photoelectrochemical performance. *J. Mater. Chem. A* **2019**, *7*, 21997–22004. [[CrossRef](#)]
27. Zhu, X.; Guan, Z.; Wang, P.; Zhang, Q.; Dai, Y.; Huang, B. Amorphous TiO_2 -modified CuBi_2O_4 Photocathode with enhanced photoelectrochemical hydrogen production activity. *Chin. J. Catal.* **2018**, *39*, 1704–1710. [[CrossRef](#)]
28. Wang, F.; Septina, W.; Chemseddine, A.; Abdi, F.F.; Friedrich, D.; Bogdanoff, P.; van de Krol, R.; Tilley, S.D.; Berglund, S.P. Gradient Self-Doped CuBi_2O_4 with Highly Improved Charge Separation Efficiency. *J. Am. Chem. Soc.* **2017**, *139*, 15094–15103. [[CrossRef](#)]
29. Shah, A.K.; Sahu, T.K.; Banik, A.; Gogoi, D.; Peela, N.R.; Qureshi, M. Reduced graphene oxide modified CuBi_2O_4 as an efficient and noble metal free photocathode for superior photoelectrochemical hydrogen production. *Sustain. Energy Fuels* **2019**, *3*, 1554–1561. [[CrossRef](#)]
30. Kang, D.; Hill, J.C.; Park, Y.; Choi, K.-S. Photoelectrochemical Properties and Photostabilities of High Surface Area CuBi_2O_4 and Ag-Doped CuBi_2O_4 Photocathodes. *Chem. Mater.* **2016**, *28*, 4331–4340. [[CrossRef](#)]
31. Lee, W.-H.; Kang, J.; Park, H.S.; Nam, K.M.; Cho, S.K. Photoelectrochemical response of Au-decorated CuBi_2O_4 photocathode in bicarbonate solution. *J. Electroanal. Chem.* **2019**, *838*, 172–177. [[CrossRef](#)]
32. Jiang, Z.; Geng, H.; Cai, X.; Mao, L.; Zhao, Y.; Gu, X. Preparation of CuBi_2O_4 photocathodes for overall water splitting under visible light irradiation. *Mater. Sci. Semicond. Process.* **2021**, *134*, 105989. [[CrossRef](#)]
33. Kim, N.-W.; Choi, B.-U.; Yu, H.; Ryu, S.; Oh, J. Formation of high-density CuBi_2O_4 thin film photocathodes with polyvinylpyrrolidone-metal interaction. *Opt. Express* **2019**, *27*, A171–A183. [[CrossRef](#)] [[PubMed](#)]
34. Reddy, D.A.; Kim, Y.; Varma, P.; Gopannagari, M.; Reddy, K.A.J.; Hong, D.H.; Song, I.; Kumar, D.P.; Kim, T.K. Inverse Opal CuBi_2O_4 Photocathodes for Robust Photoelectrochemical Water Splitting. *ACS Appl. Energy Mater.* **2022**, *5*, 6050–6058. [[CrossRef](#)]
35. Jin, J.; Hu, J.; Qu, J.; Cao, G.; Lei, Y.; Zheng, Z.; Yang, X.; Li, C.M. Reaction Kinetics of Photoelectrochemical CO_2 Reduction on a CuBi_2O_4 -Based Photocathode. *ACS Appl. Mater. Interfaces* **2022**, *14*, 17509–17519. [[CrossRef](#)]
36. Lee, S.; Cha, S.; Myung, Y.; Park, K.; Kwak, I.H.; Kwon, I.S.; Seo, J.; Lim, S.A.; Cha, E.H.; Park, J. Orthorhombic NiSe_2 Nanocrystals on Si Nanowires for Efficient Photoelectrochemical Water Splitting. *ACS Appl. Mater. Interfaces* **2018**, *10*, 33198–33204. [[CrossRef](#)] [[PubMed](#)]

37. Wang, X.-D.; Xu, Y.-F.; Chen, B.-X.; Ning, Z.; Chen, H.-Y.; Kuang, D.-B.; Su, C.-Y. 3D Cathodes of Cupric Oxide Nanosheets Coated onto Macroporous Antimony-Doped Tin Oxide for Photoelectrochemical Water Splitting. *ChemSusChem* **2016**, *9*, 3012–3018. [[CrossRef](#)] [[PubMed](#)]
38. Varunkumar, K.; Sellappan, R. Photoelectrochemical behaviour of CuBi₂O₄@MoS₂ photocathode for solar water splitting. *Mater. Chem. Phys.* **2021**, *261*, 124245. [[CrossRef](#)]
39. Choi, Y.-H.; Yang, K.D.; Kim, D.-H.; Nam, K.T.; Hong, S.-H. p-Type CuBi₂O₄ thin films prepared by flux-mediated one-pot solution process with improved structural and photoelectrochemical characteristics. *Mater. Lett.* **2017**, *188*, 192–196. [[CrossRef](#)]
40. Park, H.S.; Lee, C.-Y.; Reisner, E. Photoelectrochemical reduction of aqueous protons with a CuO|CuBi₂O₄ heterojunction under visible light irradiation. *Phys. Chem. Chem. Phys.* **2014**, *16*, 22462–22465. [[CrossRef](#)]
41. Song, A.; Plate, P.; Chemseddine, A.; Wang, F.; Abdi, F.F.; Wollgarten, M.; van de Krol, R.; Berglund, S.P. Cu:NiO as a hole-selective back contact to improve the photoelectrochemical performance of CuBi₂O₄ thin film photocathodes. *J. Mater. Chem. A* **2019**, *7*, 9183–9194. [[CrossRef](#)]
42. Monny, S.A.; Zhang, L.; Wang, Z.; Luo, B.; Konarova, M.; Du, A.; Wang, L. Fabricating highly efficient heterostructured CuBi₂O₄ photocathodes for unbiased water splitting. *J. Mater. Chem. A* **2020**, *8*, 2498–2504. [[CrossRef](#)]
43. Jeong, H.W.; Zsigmond, T.S.; Samu, G.F.; Janáky, C. Sacrificial Agent Gone Rogue: Electron-Acceptor-Induced Degradation of CsPbBr₃ Photocathodes. *ACS Energy Lett.* **2022**, *7*, 417–424. [[CrossRef](#)]
44. Liu, R.; Zheng, Z.; Spurgeon, J.; Yang, X. Enhanced photoelectrochemical water-splitting performance of semiconductors by surface passivation layers. *Energy Environ. Sci.* **2014**, *7*, 2504–2517. [[CrossRef](#)]
45. Li, J.; Griep, M.; Choi, Y.; Chu, D. Photoelectrochemical overall water splitting with textured CuBi₂O₄ as a photocathode. *Chem. Commun.* **2018**, *54*, 3331–3334. [[CrossRef](#)] [[PubMed](#)]

Disclaimer/Publisher's Note: The statements, opinions and data contained in all publications are solely those of the individual author(s) and contributor(s) and not of MDPI and/or the editor(s). MDPI and/or the editor(s) disclaim responsibility for any injury to people or property resulting from any ideas, methods, instructions or products referred to in the content.